NANO LETTERS

2001
Vol. 1, No. 10
575−579

Probing pH-Tuned Morphological Changes in Core–Shell Nanoparticle Assembly Using Atomic Force Microscopy

Mathew M. Maye, Jin Luo, Li Han, and Chuan-Jian Zhong*

Department of Chemistry, State University of New York at Binghamton, Binghamton, New York 13902

Received July 25, 2001; *Revised Manuscript Received August 1, 2001*

ABSTRACT

This paper reports novel findings of an investigation of pH-tuned morphological changes in a core–shell gold nanoparticle assembly derived from hydrogen-bonding at the encapsulating shells. Our strategy couples the selective assembly of such hydrogen-bonding-linked nanoparticles at patterned substrates with the capability of atomic force microscopy to detect the nanostructural changes in the pH-tuned interfacial process. The selective assembly on a monolayer-patterned substrate provided an ideal imaging platform with an internal standard from the unassembled areas. The detection of significant and reversible changes of both friction and height in the nanoparticle-assembled areas provided new insights into understanding of ionic fluxes and solvation effect within the nanoporous structure, which have important implications to the design of nanoparticle-based interfaces for nanostructured catalysis and molecular recognition.

Nanostructured core−shell nanoparticles are interesting because of potential applications in microelectronics, catalysis, molecular recognition, and chemical, photochemical, and biological processes.[1−5] Such nanoparticles can be broadly defined[1b] as nanoscale core and shell of different matters in close interaction, including inorganic/organic, inorganic/inorganic, organic/organic, or inorganic/biological combinations. Recent progress in two-phase synthesis[6−8] and its synthetic tailoring[9−11] has led to a variety of thiol monolayer-encapsulated metal nanoparticles or monolayer-protected clusters as monodispersing, stable, and chemically tunable building blocks in terms of size, shape, and surface properties.[2,6−11] A challenging issue is the ability to assemble the building blocks into useful materials for subsequent characterization and utilization of the nanostructured properties. Findings of place-exchange reactivity[10,11] have enabled the ability to molecularly engineer the nanostructured shell composition and functionality. Other emerging approaches, including complimentary DNA-linking,[3b,12−13] protein-linking,[14a] stepwise layer-by-layer assembly,[8,10,14−17] and a one-step exchange-cross-linking-precipitation route,[18] have also demonstrated the ability to assemble nanoparticles as platforms for addressing different technological applications. One intriguing system, which is studied in this work, involves exchanging and cross-linking of carboxylic acid functionalized alkanethiols (e.g., 11-mercaptoundecanoic acid (MUA) or 15-mercaptohexadecanoic acid (MHA)) with alkanethiolates on gold nanoparticles (2∼5 nm core sizes). The reactivity leads to the formation of the nanoparticles in a 3D network via intershell head-to-head hydrogen-bonding of the carboxylic acid terminals.[18b,c] Such a core−shell linked nanoparticle assembly is recently shown to exhibit pH-tunable ion-gating properties.[18b] The understanding of how the morphology changes in the interfacial processes is increasingly important for a precise control or manipulation of such nanostructured functional properties.

This paper reports novel findings of an investigation of the pH-tuned morphological changes in the core−shell nanoparticle assembly derived from the intershell hydrogen-bonding. Our strategy couples the selective assembly of the nanoparticles at patterned substrates with the capability of atomic force microscopy[19−22] for the detection. The selective assembly on a monolayer-patterned substrate serves the imaging platform with an internal standard, providing thus the opportunity to unravel the interfacial reactivity-morphology correlation.

The synthesis of 5-nm core-sized Au nanoparticles encapsulated with a decanethiol monolayer (Au_{5-nm}) involved the two-phase protocol[6] and a thermally activated processing route.[23] The latter converted the presynthesized 2-nm Au particles (1.9 ± 0.7 nm) to particles of 5-nm core size with high monodispersity (5.2 ± 0.3 nm).[23] Patterns of octyldecanethiol (ODT) monolayer were prepared on a gold film

* To whom correspondence should be addressed. Phone: 607-777-4605. E-mail: cjzhong@binghamton.edu.

10.1021/nl010057z CCC: $20.00
Published on Web 08/24/2001

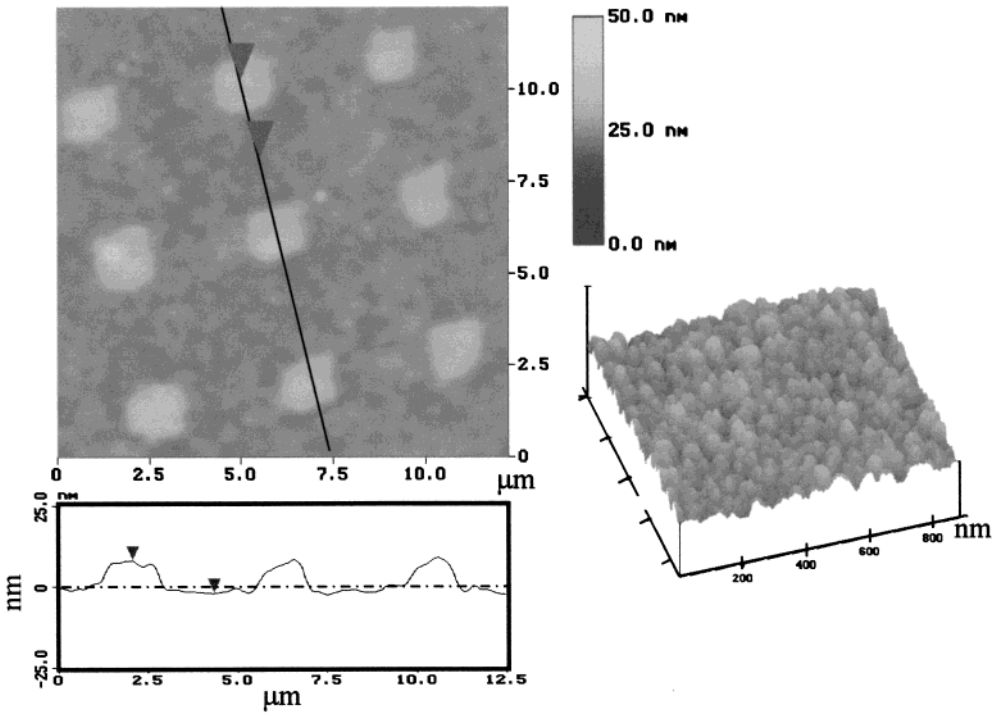

Figure 1. (A) A CM-AFM image of the selectively assembled MUA−Au_{5-nm} film on an ODT−MHA patterned surface (MHA: squares). (B) A TM-AFM image of the assembled nanoparticles (assembling time: 5 min).

substrate using microcontact stamping[24] followed by backfilling with MHA or MUA, producing 2×2 μm^2 square domains of $-CO_2H$ terminals surrounded by domains of $-CH_3$ terminals ("ODT−MHA pattern"). The MUA-linked Au_{5-nm} nanoparticle thin film (MUA−Au_{5-nm}) was prepared on the ODT−MHA patterned surface via one-step "exchanging-crosslinking-precipitation" route.[18b,c] Briefly, the monolayer-patterned substrate was vertically immersed in hexane solution of Au_{5-nm} and MUA mixed at a controlled ratio (0.02 μM Au_{5-nm} and 0.04 mM MUA in hexane). Under this condition, the shell exchanging and cross-linking led to a thin film precipitation. The thickness of the film was controlled by immersion time.[18c] The assembled MUA−Au_{5-nm} film was thoroughly rinsed with hexane. A Multimode NanoScope III was utilized for imaging the samples in both contact mode (CM) using an oxide-sharpened silicon nitride tip (~0.12 N/m) and tapping mode (TM) using a silicone tip.

Our work began with monolayer patterning for the selective assembly. Such a pattern was first confirmed by AFM imaging of both friction and topography (not shown). While the friction image of the ODT−MHA pattern showed a sharp contrast between the MHA domains (higher friction voltage) and the ODT domains surrounding them, the topography image displayed barely any height contrast between the two different domains. The former is in agreement with the fact that the friction force at the $-CO_2H$ domain is greater than the $-CH_3$ domain.[19−22] The latter is consistent with the largely identical chain length between ODT and MHA molecules.

While we have used a variety of techniques such as UV−vis, infrared reflection spectroscopy, X-ray diffraction, and quartz-crystal microbalance (QCM) to characterize the one-step assembly of MUA-linked gold nanoparticles on regular planar substrates,[18b−d] the selective assembly of such hydrogen-bonding-linked particles on the patterned substrate is demonstrated here for the first time. We note that stepwise assembly of Au nanoparticles on MUA-patterned and mercaptoethylamine-backfilled Au substrate was recently reported in which MUA serves as a pattern "inert" to colloidal Au.[15b] We also note that lithographic patterning of organic monolayers with a photolabile protection group for selectively assembling semiconducting and/or metallic nanocrystals was recently reported, which involved characterizations of the assembled nanostructures using photoluminescence and absorption spectroscopy.[25] Our approach here is to use hydrogen-bonding-active carboxylic acid groups to selectively assemble the nanoparticles as a platform for in-situ AFM probing of its morphological changes. Either an ODT−MHA patterned or an ODT patterned substrate was immersed into the hexane solution of Au_{5-nm} and MUA[18c] for the assembly of MUA−Au_{5-nm}. The latter substrate was effectively a pattern of ODT−MUA. After the MUA−Au_{5-nm} film was assembled on the patterned substrate, the assembling selectivity was examined by AFM imaging.

Figure 1 shows a CM-AFM image of an assembled MUA−Au_{5-nm} film on the patterned surface (A), and a TM-AFM image of the assembled nanoparticles (B). The topographical contrast in the image (A) indicates a selective assembly of the particles on the MHA domains. Such a preferential assembly of nanoparticles is clearly evidenced by the cross-section view that reveals that the MHA square domains are higher than the ODT domains, and by changes in friction contrast. The height was found to increase as a function of assembling time. We note, however, that for films formed at higher concentrations of nanoparticles, or for a

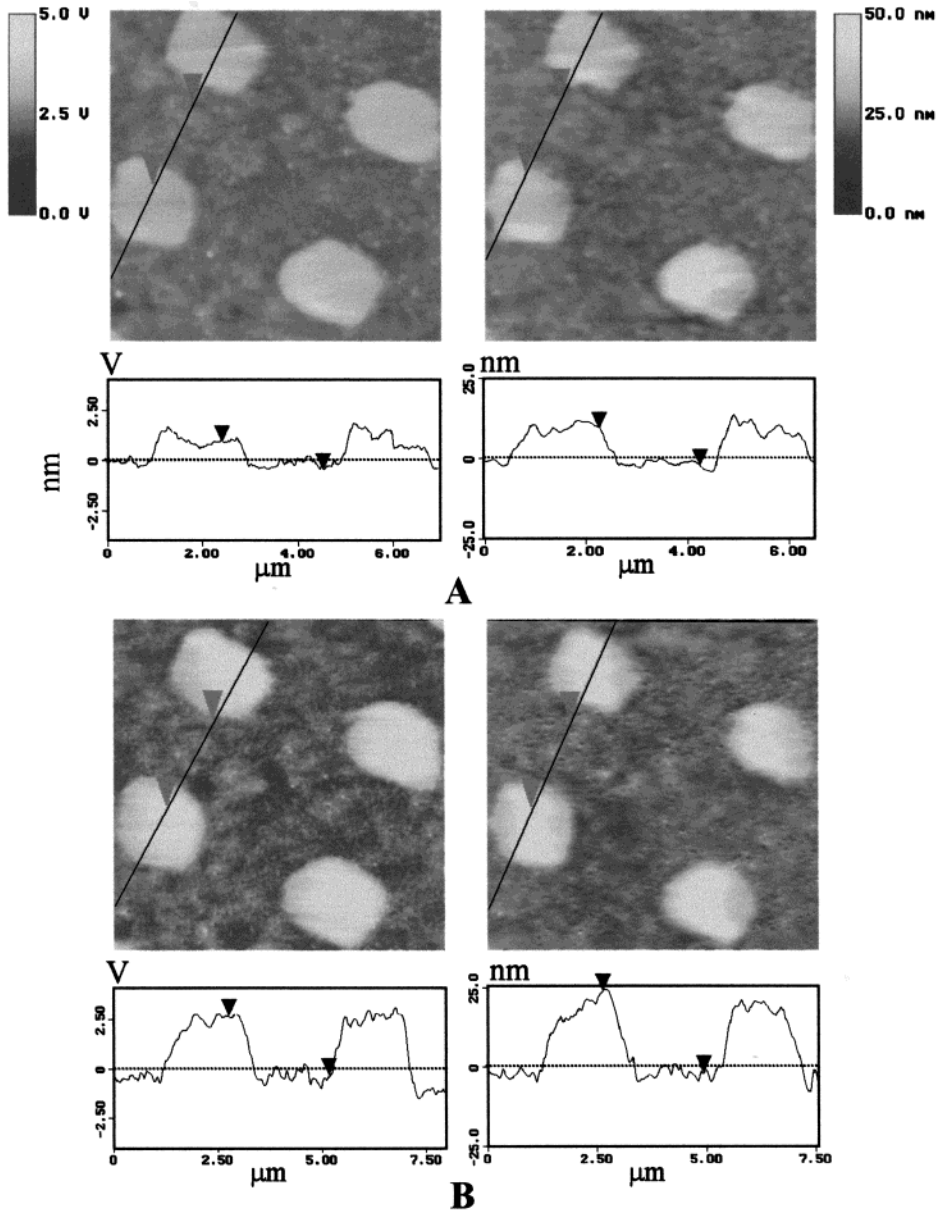

Figure 2. CM-AFM images ($8 \times 8\ \mu m^2$) of friction (left) and topography (right) for an MUA−Au_{5-nm} film assembled on ODT−MHA patterned substrate (MHA: squares) under different pHs. pH = 2 (A); pH = 11 (B).

longer assembling time, the selectivity was found to decrease and the formation of powder precipitates in the assembling vessel was also detectable.[18a,c] A detailed delineation of the parameters for the selective assembly is in progress. For the nanoparticle films assembled on the patterned substrate, height changes ranging from a few nm to ~100 nm, depending on concentrations and assembling time, were detectable, which were in close agreement with QCM data.[18c] A calculation of the head-to-head hydrogen-bonding-linked Au_{5-nm} particles in an idealized close-packing model[18b] indicated that the QCM-estimated thickness was larger than the AFM-determined thickness by a factor of 2.5. Since the AFM data for the selective assembly provided a more precise measurement of the thickness, the particles were likely packed more densely than the idealized model. The TM-AFM image (B) shows that the assembled nanoparticles are spatially isolated. The particle sizes appear larger than the core−shell nanoparticles due to tip−sample convolution, but the cross-section view reveals an average height near the expected size.

The selective assembly of the MUA−Au_{5-nm} film was then probed at different pHs in aqueous solution using CM-AFM in either a liquid drop or a fluid cell. We note that in the latter case there existed a certain change in $x-y$ scale (a factor of 1.2~1.6) due to an O-ring effect. Figure 2 presents a typical set of friction and topography images at pH 2 and 11 (A and B, respectively). The pH was adjusted using HCl or NaOH solutions. It is evident that the images maintain a clear contrast between the MUA−Au_{5-nm} domains and the unassembled domains (ODT). The friction contrast is again supportive of the lack of particles assembled on the ODT domains.

The cross-section view corresponding to the line drawn in each image provides a quantitative measure of the changes

Scheme 1. Schematic Illustration of the AFM Detection of the pH-tuned Morphological Change in the Nanoparticle Assembly

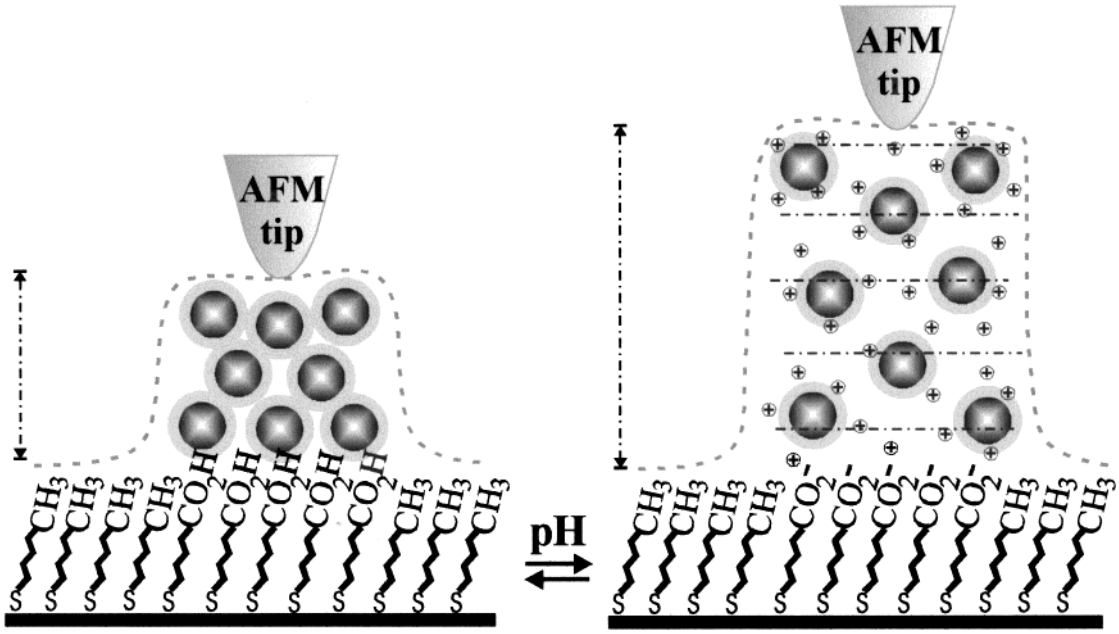

Table 1: Friction Voltage and Height Differences at Different pH for a MUA−Au_{5-nm} Film Selectively Assembled on a ODT−MHA Patterned Gold Substrate[a]

pH	friction voltage (V)	topographic height (nm)
2	1.3	10.8
7	2.8	20.1
11	3.3	24.4

[a] Based on bearing-analysis.

in friction or height. Table 1 summarizes these changes for three different pHs. The values were determined from Bearing analysis of the cross-section data, reflecting the averaging difference of 10 addresses (squares) with respect to the ODT-domain. For a comparison, the film in ambient condition (dry film) showed an average difference of 0.6 V in friction voltage and an average difference of 13.8 nm in height between the two different domains. The friction voltage is proportional to the frictional force, whereas the height value is proportional to the thickness of the assembled film. At pH = 2 (A), the difference in friction voltage was 1.3 V. In the height data, the average difference was 10.8 nm. In contrast, at pH = 11 (B), the average difference in friction voltage was 3.3 V, and the average height difference was 24.4 nm. At pH = 7, intermittent values of the friction voltage and the height were detected. Clearly, both friction voltage and topographical height were found to increase with increasing pH. The net change in friction voltage from pH 2 to 11 was about 2.0 V, whereas the net height change was about 13.6 nm. Both dependencies appear to show approximately linear relationships. Since the pH-dependence is largely reversible, the particles are insoluble in the aqueous condition, and the topographical features in the $x-y$ plane do not show a significant change, we believe that the particles do not leave the film in the above process.

The ability of detecting changes in both friction voltage and topographic height as a function of pH is remarkable. In particular, the magnitude of the height change is, to our knowledge, not reported for any hydrogen-bonding-linked nanoparticle thin film assembly. There are both qualitative and quantitative implications of our findings in terms of a mechanistic insight into the pH-tuned nanostructured interfacial reactivity. At low pH, an uncontaminated SiN_4 tip likely has −OH or $-NH_2$ groups on the tip surface,[19] whereas the nanostructured particles are linked by "head-to-head" hydrogen-bonded linkages ($-CO_2H\cdots HO_2C-$) and alkyl chains.[18b] The increase of height in an average of ∼13.6 nm from pH 2 to pH 11 is apparently much larger than the expectation simply based on the incorporation of cations into the nanoparticle layers or interparticle regions with carboxylate groups. This is because the film has only ∼4 equivalent number of nanoparticle layers (based on a correlation between QCM-estimated and AFM-determined thickness data). It is thus likely that the deprotonated MUA−Au_{5-nm} thin film "swells" due to the concurrent flux of ions and solvent molecules across the film. Assuming an idealized packing model,[18b] a net swelling of ∼13.6 nm could be roughly translated to an averaging space of ∼3 nm between two neighboring sheets of carboxylates for the swollen film. Such a swelling effect leads to an increase in volume of the film involving both the interparticle linkages and the membrane-like interfaces across the entire nanostructured assembly. The nanoparticles are held together by electrostatic binding between carboxylate groups in the film and cations from the solution. Because solvent uptake plays an important role in this process, the particles must be separated in a larger distance than that in the case of hydrogen-bonding linkage. Scheme 1 illustrates such a pH-tuned process for the AFM imaging of morphological change in the selectively assembled nanoparticle film. The detected height change is due

to the ionic and solvent fluxes into the film. As the tip scans across the interface of the solvated and electrostatically linked core−shell particles, a larger dissipation of energy is expected based on the consideration of a greater perturbation of the loosely packed nanostructure. As a result, the increased dissipation of energy leads to a greater friction force, which is detected at the higher pH.

The detection of the unusually large changes in friction and height upon pH-tuning provides new insights into the nanostructure in terms of the molecularly tunable ionic transport and ion-gating recognition properties of the film.[18b] It implies that the assembled film resembles a highly nanoporous membrane in which a considerable amount of water molecules and ions could reversibly be loaded and released by changing pH. On the basis of the ionic strengths at the two pHs, 0.01−0.001 M, the Debye length is estimated to be 3−10 nm.[26] Since the value is comparable or larger than the determined interparticle spacing (∼3 nm) in the swollen film, the electrostatic charges (CO_2^- and Na^+) are only partially screened by the diffuse ionic clouds. As such, it is possible that van der Waals forces between particles are also operative, being partially responsible for the interparticle interactions in the swollen film. Further implications of the findings to the explorations of the nanoparticle assembly for nanostructured catalysis[27] and molecular recognition[18b] will be addressed through studies of different electrolytic ions, nanocrystal core sizes, and shell structures to correlate the morphological changes with the nanostructured interfacial reactivity.

Acknowledgment. Financial support of this work is gratefully acknowledged from the American Chemical Society PRF grant, 3M, and MRS-UMRI awards. The support for AFM instrumentation is also gratefully acknowledged from the NSF-CCLI grant. We acknowledge Digital Instruments for loaner TappingMode components.

References

(1) (a) Caruso, F. *Adv. Mater*. **2001**, *13*, 11. (b) Schneider, J. J. *Adv. Mater*. **2001**, *13*, 529. (c) Shipway, A. N.; Katz, E.; Willner, I. *ChemPhysChem.* **2000**, *1*, 18.

(2) Templeton, A. C.; Wuelfing, W. P.; Murray, R. W., *Acc. Chem. Res*. **2000** *33*, 27.

(3) (a) Link, S.; El-Sayed, M. A. *Int. Rev. Phys. Chem*. **2000**, *19*, 409. (b) Storhoff, J. J.; Mirkin, C. *Chem. Rev.* **1999**, *99*, 1849.

(4) Peng, X.; Schlamp, M. C.; Kadavanich, A. V.; Alivisatos, A. P. *J. Am. Chem. Soc.* **1997**, *119*, 7019.

(5) (a) Whetten, R. L.; Shafigulin, M. N.; Khoury, J. T.; Schaff, T. G.; Vezmar, I.; Alvarez, M. M.; Wilkinson, A. *Acc. Chem. Res.* **1999**, *32*, 397. (b) Whetten, R. L.; Khoury, J. T.; Alvarez, M. M.; Murthy, S.; Vezmar, L.; Wang, Z. L.; Stephens, P. W.; Cleveland, C. L.; Luedtke, W. D.; Landman, U. *Adv. Mater*. **1996**, *8*, 428.

(6) (a) Brust, M.; Walker, M.; Bethell, D.; Schiffrin, D. J.; Whyman, R. *J. C. S. Chem. Commun*. **1994**, 801. (b) Kiely, C. J.; Fink, J.; Brust, M.; Bethell, D.; Schiffrin, D. J. *Nature* **1998**, *396*, 444.

(7) Brust, M.; Fink, J.; Bethell, D.; Schiffrin, D. J.; Kiely, C. *J. C. S. Chem. Commun.* **1995**, 1655.

(8) Bethell, D.; Brust, M.; Schiffrin, D. J.; Kiely, C. *J. Electroanal. Chem.* **1996**, *409*, 137.

(9) Hostetler, M. J.; Wingate, J. E.; Zhong, C. J.; Harris, J. E.; Vachet, R. W.; Clark, M. R.; Londono, J. D.; Green, S. J, Stokes, J. J.; Wignall, G. D.; Glish, G. L.; Porter, M. D.; Evans, N. D.; Murray, R. W. *Langmuir* **1998**, *14*, 17.

(10) Hostetler, M. J.; Green, S. J.; Stokes, J. J.; Murray, R. W. *J. Am. Chem. Soc*. **1996**, *118*, 4212.

(11) (a) Templeton, A. C.; Hostetler, M. J.; Kraft, C. T.; Murray, R. W. *J. Am. Chem. Soc*. **1998**, *120*, 1906. (b) Ingram, R. S.; Hostetler, M. J.; Murray, R. W. *J. Am. Chem. Soc*. **1997**, *119*, 9175. (c) Hostetler, M. J.; Templeton, A. C.; Murray, R. W. *Langmuir* **1999**, *15*, 3782. (d) Templeton, A. C.; Hostetler, M. J.; Warmoth, E. K.; Chen, S.; Hartshorn, C. M.; Krishnamurthy, V. M.; Forbes, M. D. E.; Murray, R. W. *J. Am. Chem. Soc*. **1998**, *120*, 4845.

(12) (a) Mirkin, C.; Letsinger, R. L.; Mucic, R. C.; Storhoff, J. J. *Nature* **1996**, *382*, 607. (b) Elghanian, R.; Storhoff, J. J.; Mucic, R. C.; Letsinger, R. L.; Mirkin, C. A. *Science* **1997**, *277*, 1078.

(13) (a) Mbindyo, J. K. N.; Reiss, B. D.; Martin, B. R.; Keating, C. D.; Natan, M. J.; Mallouk, T. E. *Adv. Mater*. **2001**, *13*, 249. (b) Loweth, C. J.; Caldwell, W. B.; Peng, X. G.; Alivisatos, A. P.; Schultz, P. G. *Angew. Chem., Int. Ed. Engl*. **1999**, *38*, 1808.

(14) (a) Mann, S.; Shenton, W.; Li, M.; Connolly, S.; Fitzmaurice, D. *Adv. Mater*. **2000**, *12*, 147. (b) Zheng, J. W.; Zhu, Z. H.; Chen, H. F.; Liu, Z. F. *Langmuir* **2000**, *16*, 4409.

(15) (a) Musick, M. D.; Pena, D. J.; Botsko, S. L.; McEvoy, T. M.; Richardson, J. N.; Natan, M. J. *Langmuir* **1999**, *15*, 844. (b) Musick, M. D.; Keating, C. D.; Lyon, L. A.; Botsko, S. L.; Pena, D. J.; Holliway, W. D.; McEvoy, T. M.; Richardson, J. N.; Natan, M. J. *Chem. Mater*. **2000**, *12*, 2869.

(16) (a) Kiely, C. J.; Fink, J.; Zheng, J. G.; Brust, M.; Bethell, D.; Schiffrin, D. J. *Adv. Mater*. **2000**, *12*, 640. (b) Baum, T.; Bethell, D.; Brust, M.; Schiffrin, D. J. *Langmuir* **1985**, *15*, 866.

(17) (a) Zamborini, F. P.; Hicks, J. F.; Murray, R. W. *J. Am. Chem. Soc.* **2000**, *122*, 4514. (b) Templeton, A. C.; Zamborini, F. P.; Wuelfing, W. P.; Murray, R. W. *Langmuir* **2000**, *16*, 6682. (c) Wuelfing, W. P.; Zamborini, F. P.; Templeton, A. C.; Wen, X. G.; Yoon, H.; Murray, R. W. *Chem. Mater*. **2001**, *13*, 87.

(18) (a) Leibowitz, F. L.; Zheng, W. X.; Maye, M. M.; Zhong, C. J. *Anal. Chem.* **1999**, *71*, 5076. (b) Zheng, W. X.; Maye, M. M.; Leibowitz, F. L.; Zhong, C. J. *Anal. Chem.* **2000,** *72*, 2190. (c) Han, L.; Maye, M. M.; Leibowitz, F. L.; Ly, N. K.; Zhong, C. J. *J. Mater. Chem*. **2001**, *11*, 1259. (d) Han, L.; Maye, M. M.; Zhong, C. J. In *Anisotropic Nanoparticles − Synthesis, Characterization, and Applications*; Lyon, L. A., Keating, C., Searson, P. C., Stranick, S., Eds.; Materials Research Society, Vol. 635, C4.5, 2001. (e) Zhang, F. X.; Zheng, W. X.; Maye, M. M.; Lou, Y.; Han, L.; Zhong, C. J. *Langmuir* **2000**, *16*, 9639.

(19) Takano, H.; Kenseth, J. R.; Wong, S.-S.; O'Brien, J. C.; Porter, M. D. *Chem. Rev.* **1999**, *99*, 2845.

(20) (a) Green, J.-B. D.; McDermott, M. T.; Porter, M. D.; Siperko, L. M. *J. Phys. Chem.* **1995**, *99*, 10960. (b) Wong, S.-S.; Takano, H.; Porter, M. D. *Anal. Chem.* **1935**, *70*, 5209. (c) Jones, V. W.; Kenseth, J. R.; Porter, M. D.; Mosher, C. L.; Henderson, E. *Anal. Chem.* **1935**, *70*, 1233. (d) O'Brien, J. C.; Stickney, J. T.; Porter, M. D. *J. Am. Chem. Soc.* **2000**, *122*, 5004.

(21) (a) Finot, M. O.; McDermott, M. T. *J. Am. Chem. Soc.* **1997**, *1*199, 8564. (b) Kiema, G. K.; Fitzpatrick, G.; McDermott, M. T. *Anal. Chem*. **1999**, *71*, 4306.

(22) (a) A Frisbie, C. D.; Rozsnyai, L. F.; Noy, A.; Wrighton, M. S.; Lieber, C. M. *Science* **1994**, *26*5, 2071. (b) Noy, A.; Frisbie, C. D.; Rozsnyai, L. F.; Wrighton, M. S.; Lieber, C. M. *J. Am. Chem. Soc.* **1995**, *117*, 7943.

(23) (a) Maye, M. M.; Zheng, W. X.; Leibowitz, F. L.; Ly, N. K.; Zhong, C. J. *Langmuir* **2000**, *16*, 490. (b) Maye, M. M.; Zhong, C. J. *J. Mater. Chem.* **2000**, *10*, 1895.

(24) (a) Kumar, A.; Biebuyck, H. A.; Whitesides, G. M. *Langmuir* **1994**, *10*, 1498. (b) Delamarche, E.; Schmid, H.; Bietsch, A.; Larsen, N. B.; Rothuizen, H.; Michel, B.; Biebuyck, H. *J. Phys. Chem. B*. **1998**, *102*, 3324.

(25) Vossmeyer, T.; Jia, S.; Delonno, E.; Diehl, M. R.; Kim, S. H.; Peng, X.; Alivisatos, A. P.; Heath, J. R. *J. Appl. Phys.* **1998**, *84*, 3664.

(26) Israelachvili, J. *Intermolecular and Surface Forces*, 2nd Ed., Academic Press: New York, 1992; p 238.

(27) (a) Maye, M. M.; Lou Y.; Zhong, C. J. *Langmuir* **2000,** *16*, 7520. (b) Lou, Y.; Maye, M. M.; Han, L.; Luo, J.; Zhong, C. J. *Chem. Commun.* **2001**, *5*, 473.

NL010057Z